Supporting Information to

# Soft-templated, Mesoporous Co$_3$O$_4$ Thin Films for Electrocatalysis of the Oxygen Evolution Reaction

*Qingyang Wu†, Maximilian Mellin†, Stefan Lauterbach‡, Chuanmu Tian†, Christian Dietz§, Jan P. Hofmann†, and Marcus Einert†\**

†Surface Science Laboratory, Department of Materials and Earth Sciences, Technical University of Darmstadt, Otto-Berndt-Strasse 3, 64287 Darmstadt, Germany;

‡Institute for Applied Geosciences, Geomaterial Science, Technical University of Darmstadt, Schnittspahnstrasse 9, 64287 Darmstadt, Germany

§Institute of Material Science, Physics of Surfaces, Technical University of Darmstadt, Peter-Gruenberg-Strasse 2, 64287 Darmstadt, Germany

**Corresponding Author**

*E-mail: Dr. M. Einert: meinert@surface.tu-darmstadt.de
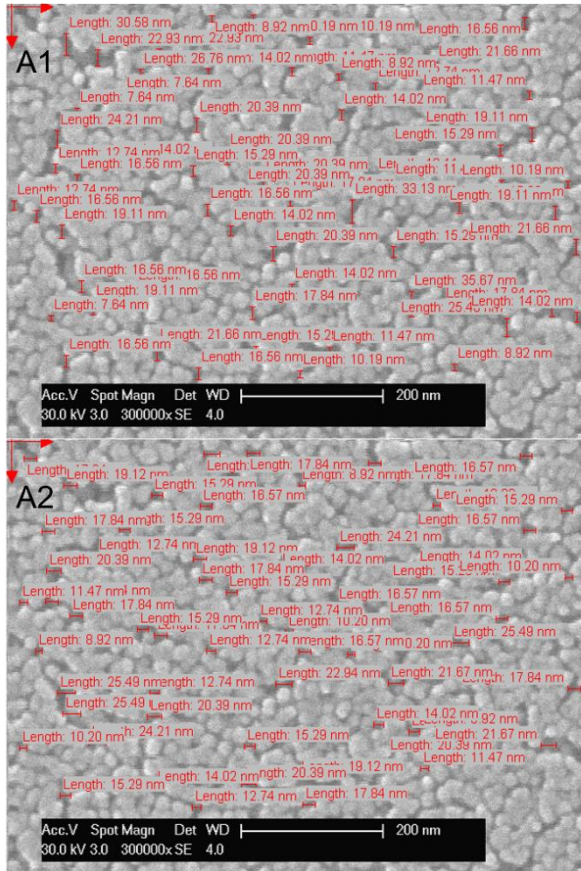
Phone: +49 6151 16-20770

**Figure S1**. Histograms B1 and B2 of pore diameters in y- and x-direction, respectively, derived from SEM analysis A1 and A2 with Weibull distribution lines determined for a meso-$Co_3O_4$ thin film.
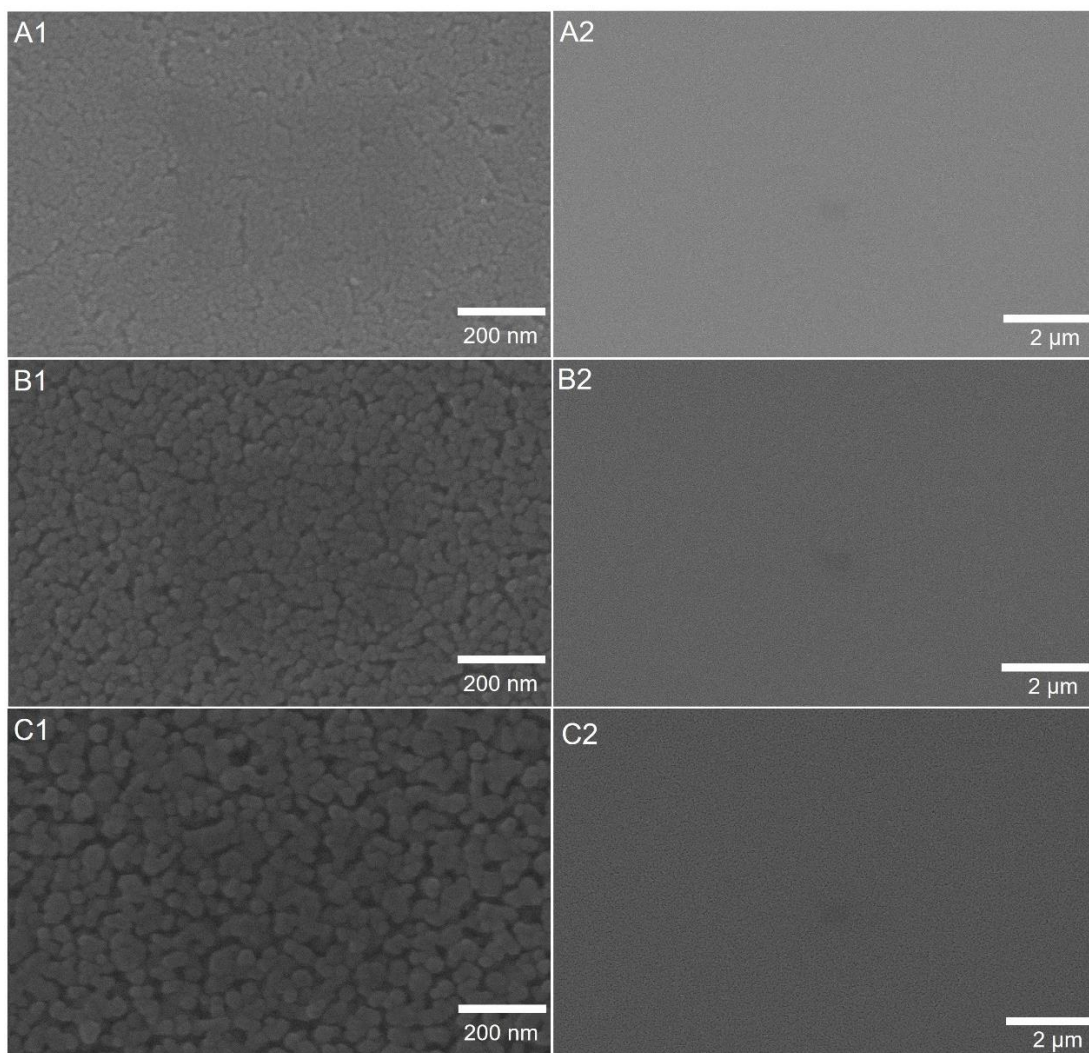
**Figure S2.** SEM images of the meso-$Co_3O_4$ thin films annealed at A 1-2) 400 °C, B 1-2) 500 °C, and C 1-2) 600 °C for 30 min in air measured at distinct magnifications.
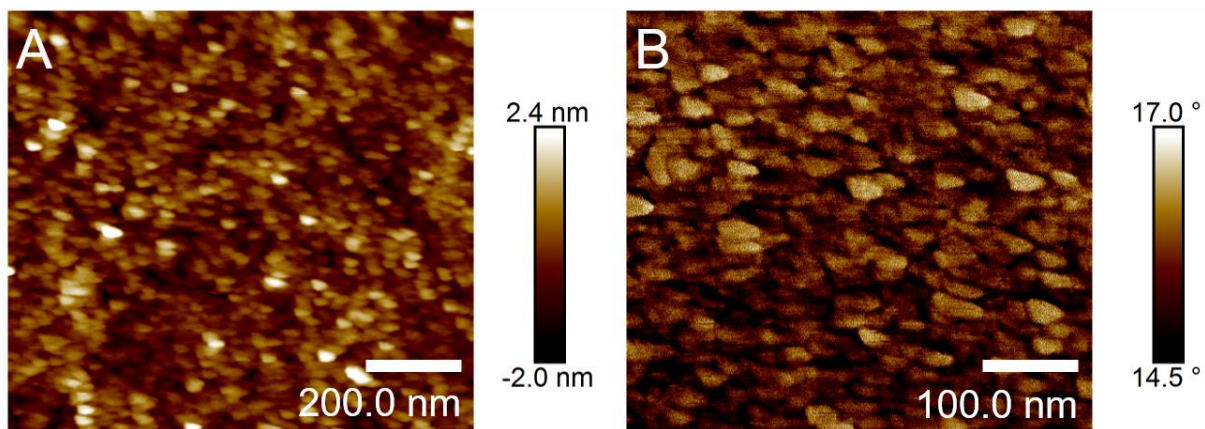
**Figure S3.** AFM analysis of the surface of the meso-$Co_3O_4$ thin film sample prepared at 300 °C detected in A) topographic and B) phase-mode including a color code visualizing the height difference and the phase shift of the cantilever, respectively.
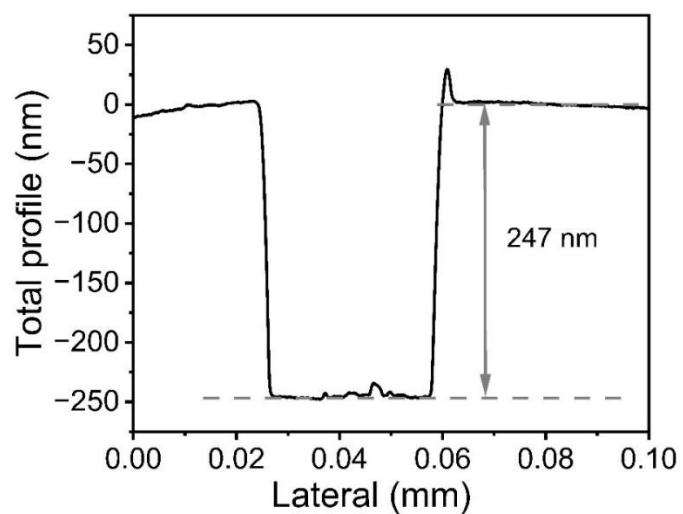


**Figure S4.** Determination of the film thickness of meso-$Co_3O_4$ thin films prepared via dip-coating on a silicon substrate by profilometry.
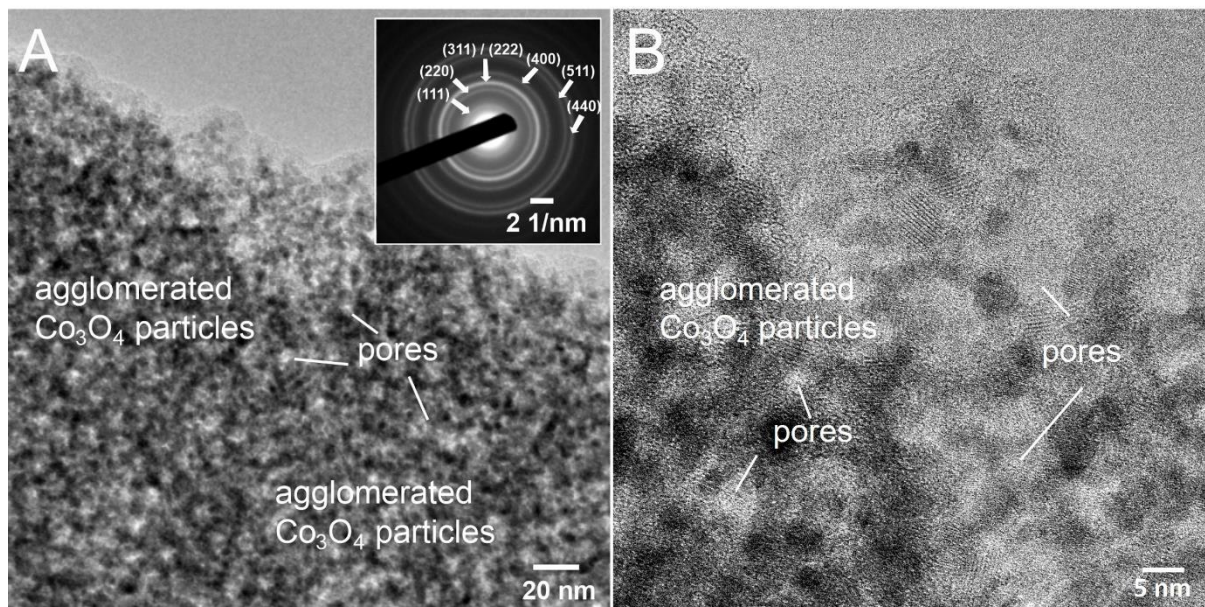
**Figure S5**. A) Bright-field TEM with inset showing SAED patterns from the bulk area, which were indexed in agreement with the cubic spinel phase. B) HR-TEM image of meso-$Co_3O_4$ demonstrating mesopores and agglomerated $Co_3O_4$ nanoparticles.
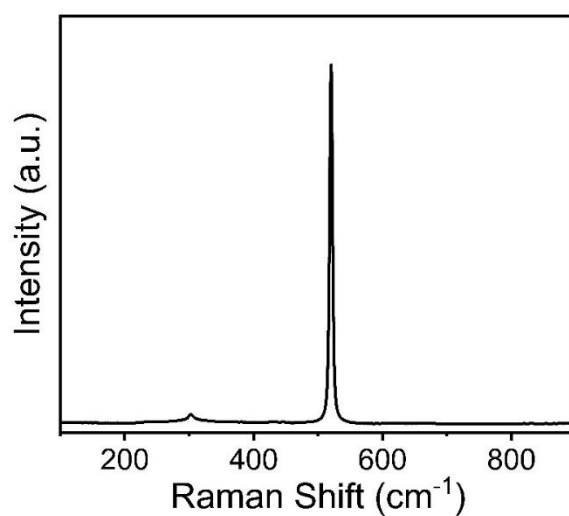


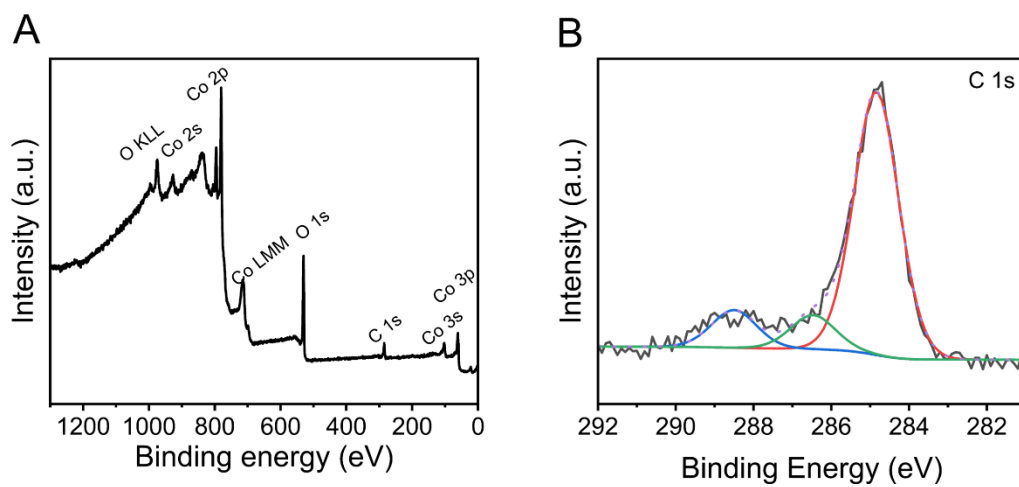**Figure S6**. Raman spectrum of a pristine silicon substrate.

**Figure S7.** A) XPS survey spectrum and B) C 1s spectrum of meso-$Co_3O_4$ at 300 °C calcined for 30 min.
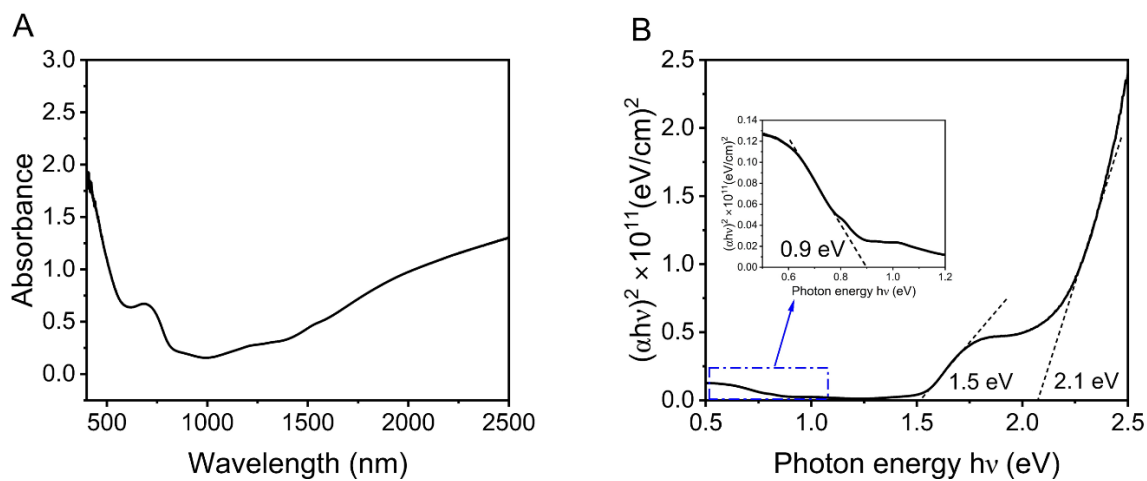


**Figure S8**.A) Absorbance spectra for the meso-$Co_3O_4$ thin film prepared at 300 °C and calcined for 30 min and B) the corresponding Tauc plots for a direct optical transition.
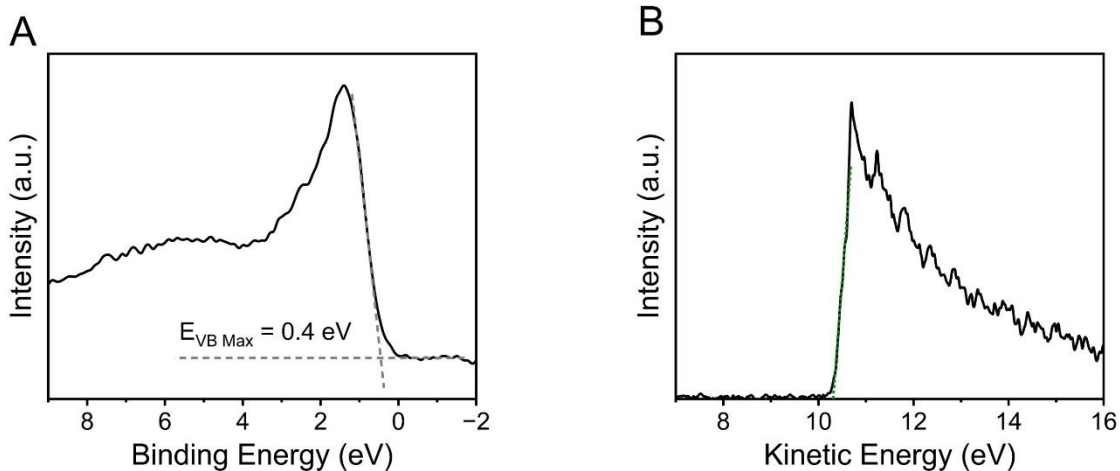
**Figure S9**. Evaluation of the A) valence band maximum by graphical linear fitting of the data for binding energies between 0 eV and 1 eV, and B) the secondary cutoff region of the XPS spectrum of meso-$Co_3O_4$, which was collected with a photoelectron take-off angle of 90° and with a –6 V bias applied to the sample.



**Figure S10.** Scan rate-dependent cyclic voltammetry curves recorded for A) meso- and B) dense $Co_3O_4$ thin films at distinct scan rates ranging from 20 mV/s to 200 mV/s.

**Figure S11.** A SEM image of the meso-$Co_3O_4$ thin film deposited on an FTO substrate and after electrochemical analysis (which was CV, LSV, DCV, and EIS, see experimental section of the manuscript).
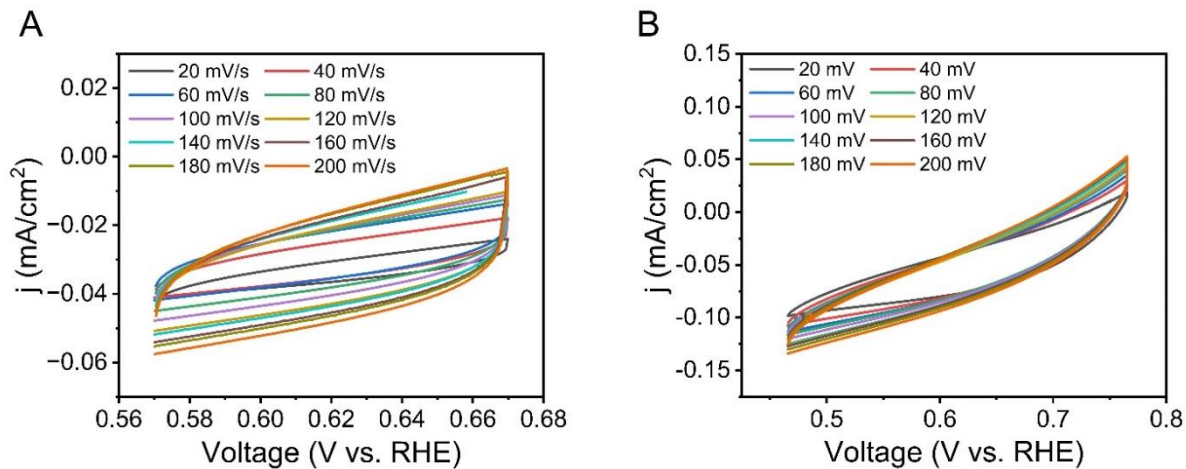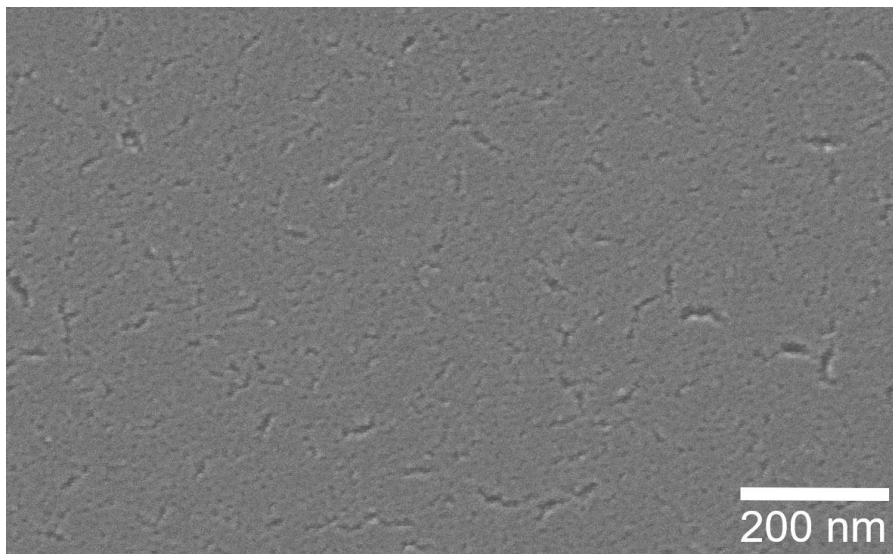
**Table S1.** OER performances for nanostructured cobalt oxides investigated in alkaline solutions.

| Catalyst | Synthesis method | Electrolyte | Substrate | Over-potential ($\eta$) at 10 mA/cm$^2$ (mV) | Onset potential (V vs. RHE) | Tafel slope (mV/ dec) | Refer-ence |
|---|---|---|---|---|---|---|---|
| $Co_3O_4$ nanosheets/nano particles/ nanospheres | Hydrothermal | 1 M KOH | glassy carbon | 342/ 350/ 448 | 1.52/ 1.53/ 1.57 | 80/ 84/ 99 | 1 |
| Mesoporous $Co_3O_4$ | Hard templating from KIT-6 mesoporous silica aging at 35 °C and 100 °C | 1 M KOH | glassy carbon | 411 (at 35 mA) 426 (100 mA) | 1.45 (35) 1.48 (100) | 60-70 | 2 |
| Mesoporous $Co_3O_4$ nanoflakes | Microwave-assisted hydrothermal and low-temperature conversion | 1 M KOH | glass carbon | 380 | 1.45 | 48 | 3 |
| Sub-5 nm $Co_3O_4$ nanoparticles | Pulsed laser fragmentation in liquid (PLFL) | 1 M KOH | Glass carbon | 400 | 1.55 | 52 | 4 |
| $Co_3O_4$ Nanowires | Thermal annealing of CoCH nanowires | 1 M KOH | Carbon fiber paper | ~330 | 1.5 | 62 | 5 |
| Cubic $Co_3O_4$ nanoparticles | Electrodeposition | 1 M KOH | Ni foam | 328 - 382 | - | - | 6 |
| $Co_3O_4$ nanocrystals | Thermal Decomposition | 1 M KOH | Carbon fiber papers | 320 | 1.52 | 101 | 7 |
| $Co_3O_4$ nanofibers | electrospinning | 1 M KOH | Fluorine doped tin oxide (FTO) | 293 | 1.42 | 60.5 | 8 |
| Two dimensional (2D) porous $Co_3O_4$ nanosheets | Graphene oxide templating | 1 M KOH | Mixtures of active material, carbon black, and sodium alginate | 368 | 1.48 | 59 | 9 |
| $Co_3O_4$ nanoflowers | Hydrothermal | 1 M KOH | Carbon cloth | 297 | ~1.38 | 79.1 | 10 |
| Mesoporous $Co_3O_4$ | Sol-gel | 0.1 M KOH | Pyrolytic graphite (PG) carbon | ~390 | 1.55 | 74.3 | 11 |
| $Co_3O_4$ catalyst | Sol-gel | 1 M KOH | Pyrex glass | ~450 | ~1.48 | - | 12 |
| Mesoporous $Co_3O_4$ thin films | Sol-gel, dip-coating | 1 M KOH | FTO | 335 | 1.5 | 59 | **This work** |

## References

1       S. Liu, R. Zhang, W. Lv, F. Kong and W. Wang, *Int. J. Electrochem. Sci.*, 2018, 3843–3854.

2       Y. J. Sa, K. Kwon, J. Y. Cheon, F. Kleitz and S. H. Joo, *J. Mater. Chem. A*, 2013, **1**, 9992.

3       S. Chen, Y. Zhao, B. Sun, Z. Ao, X. Xie, Y. Wei and G. Wang, *ACS Appl. Mater. Interfaces*, 2015, **7**, 3306–3313.

4       M. Yu, F. Waag, C. K. Chan, C. Weidenthaler, S. Barcikowski and H. Tüysüz, *ChemSusChem*, 2020, **13**, 520–528.

5       H. Xia, Z. Huang, C. Lv and C. Zhang, *ACS Catal.*, 2017, **7**, 8205–8213.

6       A. J. Esswein, M. J. McMurdo, P. N. Ross, A. T. Bell and T. D. Tilley, *J. Phys. Chem. C*, 2009, **113**, 15068–15072.

7       S. Du, Z. Ren, J. Zhang, J. Wu, W. Xi, J. Zhu and H. Fu, *Chem. Commun.*, 2015, **51**, 8066–8069.

8       A. Aljabour, *ChemistrySelect*, 2020, **5**, 7482–7487.

9       Z. Li, X.-Y. Yu and U. Paik, *J. Power Sources*, 2016, **310**, 41–46.

10      J. Du, C. Li and Q. Tang, *Electrochimica Acta*, 2020, **331**, 135456.

11      W. Song, Z. Ren, S.-Y. Chen, Y. Meng, S. Biswas, P. Nandi, H. A. Elsen, P.-X. Gao and S. L. Suib, *ACS Appl. Mater. Interfaces*, 2016, **8**, 20802–20813.

12      M. El Baydi, G. Poillerat, J.-L. Rehspringer, J. L. Gautier, J.-F. Koenig and P. Chartier, *J. Solid State Chem.*, 1994, **109**, 281–288.